IEEE Robotics and Automation Letters (RA-L) paper, presented at ICRA 2026, Vienna, Austria. Cite as RA-L paper.

High-Speed Scooping through Dynamic Manipulation: Model and Practice

Hyeonje Cha, Inho Lee, and Jungwon Seo

***Abstract*—This study introduces a robotic high-speed scooping technique, an effective solution for rapidly picking thin objects from a hard support surface. High-speed scooping involves dynamic and impactful manipulation using a two-fingered gripper. One digit dynamically penetrates beneath the object lying on a support surface while the other digit helps form a cage and subsequently secures a firm grip. This entire process is executed within a fractional-second time frame. We develop a theoretical model of manipulation for high-speed scooping and implement it using our custom direct-drive gripper designed for enhanced environment-adaptability. Extensive experiments verify the viability of our high-speed scooping approach.**

***Index Terms*—In-Hand Manipulation, Grasping, Dexterous Manipulation**

I. Introduction

HANDLING thin objects presents significant challenges for robots, particularly with items such as plastic cards, coins, small electronic parts, and similar objects. Specifically, when these objects rest on a hard surface, reachability is highly constrained, leaving only the top face readily accessible. This creates a demanding scenario for standard multi-fingered grippers, which primarily rely on unilateral contact forces and friction. Suction-based gripping, capable of exerting bilateral contact forces, has been a practical solution to this challenge, as demonstrated in the Amazon Picking Challenge [1]. However, suction grippers often need to be used alongside a multi-fingered gripper (see [1] again), due to limitations such as sensitivity to surface conditions [2], [3].

In this study, we establish a novel dynamic manipulation model for quickly scooping objects off from a hard surface using a multi-fingered gripper. We implement this manipulation model and verify its effectiveness and practicality. Fig. 1a illustrates the rapid scooping process using our custom two-fingered gripper, which uses direct-drive actuation. The process begins with the gripper, attached to a motion-controlled arm, being slammed onto the surface where the object is located. Upon detecting the collision with the surface, the gripper performs a dynamic scooping action (Fig. 1b): one digit, the thumb, is inserted between the object and the surface while the other, the finger, pushes down on the object. This entire physical interaction is executed within a subsecond time interval (Fig. 1a), without needing to stop the arm's motion.

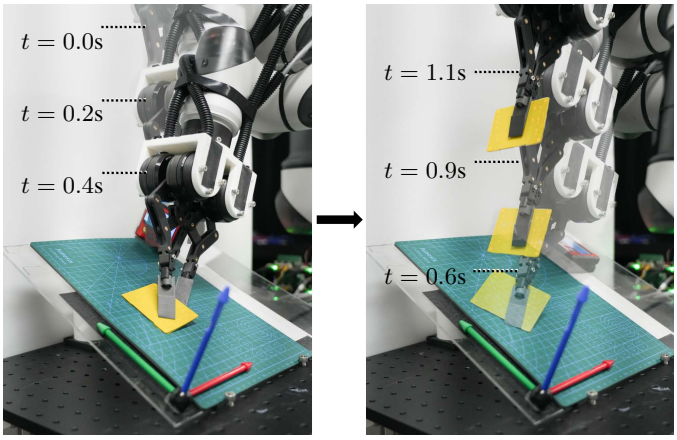

(a)

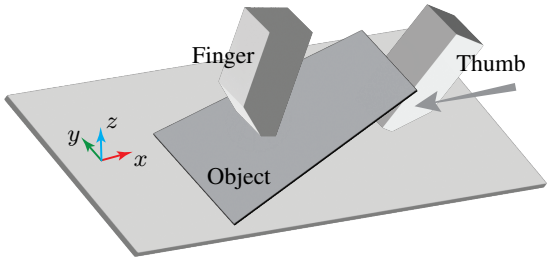

(b)

Fig. 1. (a) High-speed scooping. The robot with a two-fingered gripper is quickly scooping a plastic card resting on a hard surface. (b) Schematic of the high-speed scooping technique. The gripper's working plane, the xz-plane, is assumed to be perpendicular to the ground surface, the xy-plane. In practice, as can be noticed in (a), this assumption can be mitigated by our finger mechanism, to be addressed later in this paper.

We refer to the presented picking technique as "high-speed scooping." This term was first introduced in our recent conference presentation [4], which focused on low-level engineering aspects addressing how to achieve high-speed scooping. In this article, we explore the 'why' behind the process by establishing a new theoretical model for high-speed scooping and present an updated implementation of the technique, incorporating enhanced design features such as swivel fingertips to improve adaptability to uncertain environ-

Manuscript received: August, 15, 2024; Revised November, 13, 2024; Accepted December, 9, 2024.

This paper was recommended for publication by Editor Júlia Borràs Sol upon evaluation of the Associate Editor and Reviewers' comments (*Corresponding author: Jungwon Seo*). This work was supported by the Ministry of Trade, Industry, and Energy (MOTIE), Korea, under RS-2024-00422269 (Alchemist Project Program) and RS-2024-00406796 (KIAT HRD Program for Industrial Innovation); BK21FOUR, Creative Human Resource Education and Research Programs for ICT Convergence in the 4th Industrial Revolution; New Faculty Research Grant of Pusan National University 2022.

The authors are with Department of Electronic Engineering, Pusan National University, Busan 46241, Republic of Korea. {chahyun9823, inholee8, junseo.kr}@pusan.ac.kr

Digital Object Identifier (DOI): see top of this page.

IEEE Robotics and Automation Letters (RA-L) paper, presented at ICRA 2026, Vienna, Austria. Cite as RA-L paper.

mental conditions. Additionally, we provide a new series of experiments to support the hypotheses derived from the new manipulation model and to reconfirm the empirical feasibility and reproducibility of high-speed scooping.

This paper is organized as follows. Sec. II introduces related studies. In Sec. III, we address the dynamic manipulation model of high-speed scooping. Sec. IV and V presents an implementation of high-speed scooping and a series of experiments, respectively.

II. Related Work

This work focuses on dynamic manipulation, which considers the object's dynamics during handling. Early examples include part reorientation by tray tilting [5] and robot jugglers [6]. The study in [7] explored the control and planning of planar dynamic manipulation (extended to three dimensions in [8]), showcasing various dynamic tasks with a simple robot system. Low-dimensional models like the acrobot and cart-pole have been instrumental in solving complex dynamic manipulation problems, as demonstrated in [9] with cooperative swinging manipulation. Recently, dynamic manipulation has been showcased in tasks such as within-hand repositioning [10], learning-based manipulation of tossing [11], and object transport by rock-and-walk manipulation [12]. Dynamics has also been pivotal in the study of robot locomotion. For example in [13], passive dynamic walking is introduced as a gravity-driven dynamic process without active control. This has been extended in many directions including [14] presenting a bipedal passive walker with knee flexion. In this presented work, we apply dynamic manipulation to enable robots to acquire objects in an environment-adaptive manner. Our previous studies demonstrate the feasibility of this approach for both rigid [4] and flexible [15] objects.

The situation we address in this study–manipulation for object acquisition under physical environment constraints–has received multi-faceted attention in the literature. Design-oriented approaches, such as the incorporation of mechanical compliance and underactuation, can be seen in [16]–[18]. In terms of planning, [19] presents an optimization-based planning algorithm for scooping objects in contact with external surfaces. Recently, learning-based approaches [20] have proved effective in addressing environmental constraints. Examples include [21], which introduces self-supervised learning to leverage environmental features for grasping objects, and [22], which presents a reinforcement learning method that derives sequential actions for grasping objects occluded by external obstacles. The solution presented in this study employs a physics-based model and a gripper designed to operate compliantly.

To implement our high-speed scooping technique, we design a gripper employing direct-drive actuation [23], avoiding the use of high reduction ratio transmissions. While the benefits of direct-drive (for example, enhanced sensing due to proprioceptive feedback [24]) have been recognized for decades, its application in manipulation tasks was limited by the unavailability of suitable actuators. [25], [26] have demonstrated examples of direct-drive robotic grippers. In the field of robotic locomotion, which typically faces fewer spatial constraints than manipulation, direct-drive actuation is well-suited for adaptive multi-modal gaiting [27]. To mitigate certain limitations of direct drive, quasi-direct-drive actuation [28] offers an effective alternative. Our direct-drive gripper operates using impedance control, also known as indirect force control. This approach configures a robot to mimic a tailored second-order mechanical system, responding as intended to external forces. Foundational research in this control method is detailed in [29].

III. Model of High-Speed Scooping

This section establishes the model of dynamic manipulation for high-speed scooping, composed of two sequential stages: dynamic strike and post-strike caging. We initially assume that, in the schematic of object scooping depicted in Fig. 1b, (1) any motions of the object out of the xz-plane can effectively be suppressed and (2) the workplane of the gripper is represented by the xz-plane. This assumption allows us to focus on the planar situation within the xz-plane shown in Fig. 2a. Considering target objects that are symmetric about that plane, which still covers a variety of practical objects, provides justification for this assumption.

A. Dynamic Strike by Thumb

In the planar setup of Fig. 2a, an object to scoop is represented as a line segment lying on a flat, level ground surface. First, the object is struck by a gripper's flat thumb moving at a sufficiently high velocity $\mathbf{v}$ (recall Fig. 1), imparting enough momentum for dynamic effects to dominate over quasistatic (or purely static) phenomena. Note that in Fig. 2a we consider an observer moving with the thumb, so the object appears to approach the stationary thumb with velocity $\mathbf{v}$. We will employ rigid body mechanics to analyze this situation.

When the object is struck by the thumb (Fig. 2b), the contact between the object and corner C, formed by the thumb and the ground surface, will occur within a very brief time interval Δt. Despite this short duration, the average impulsive force $\mathbf{C}_{\text{avg}}$ exerted by the corner can be significantly high, resulting in a substantial impulse $\mathbf{C}_{\text{avg}}\Delta t = \int \mathbf{C}\mathrm{d}t$. Any other non-impulsive forces, such as the weight $\mathbf{W}$ of the object and the reaction $\mathbf{G}$ at the other end of the object indicated with a light blue color in Fig. 2b, can be disregarded due to their insignificant impulse. Now, the question arises: how will the impact alter the motion of the object?

To address this question, we examine the object's angular momentum about C, denoted $\mathbf{H}_C$. Before the impact (Fig. 2a), $\mathbf{H}_C$ represents the moment of the object's linear momentum $m\mathbf{v}$ about C (m is the mass of the object) and is therefore zero, as the vector is in line with the linear object due to its zero thickness. After the impact (Fig. 2c), the twist of the object $[\boldsymbol{\omega} \quad \mathbf{v}']^T$ must be determined so that $\mathbf{H}_C$ equals zero again, as $\mathbf{H}_C$ is preserved despite the collision, in which the only significant impulse $\mathbf{C}_{\text{avg}}\Delta t$ is exerted at C. This suggests that $\boldsymbol{\omega}$ and $\mathbf{v}'$ are related by

$$\mathbf{H}_C = I\boldsymbol{\omega} + \mathbf{r}_C \times m\mathbf{v}' = \mathbf{0} \tag{1}$$

IEEE Robotics and Automation Letters (RA-L) paper, presented at ICRA 2026, Vienna, Austria. Cite as RA-L paper.

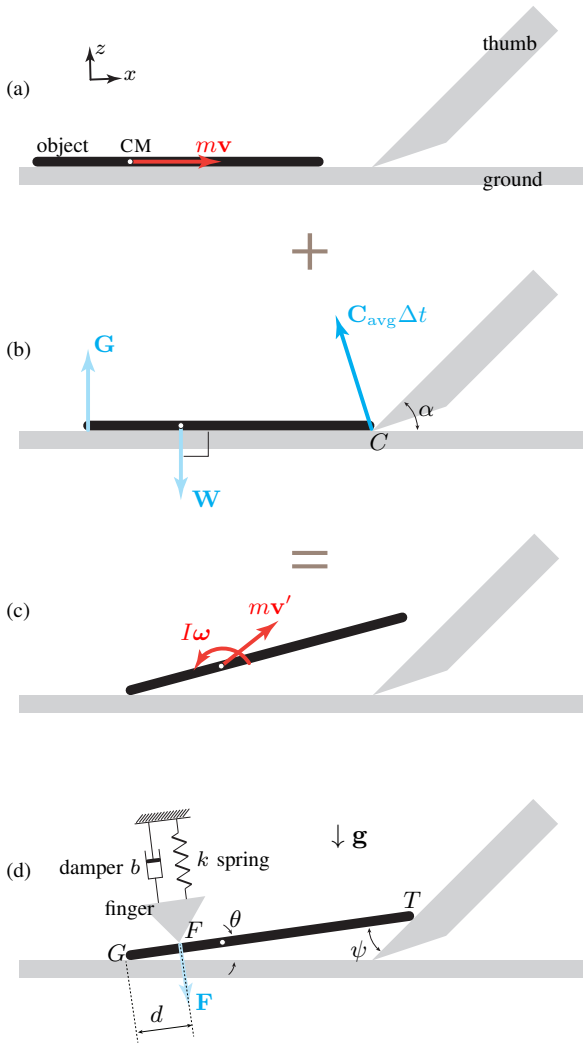

Fig. 2. (a) Planar manipulation setup. The object and thumb are about to collide. The object's linear momentum vector $m\mathbf{v}$ is attached at the mass center denoted CM. (b) System of forces during the collision: $\mathbf{G}$ (regarded non-impulsive), $\mathbf{C}$ by contact and $\mathbf{W}$ (regarded non-impulsive) by gravity. (c) System of the object's momenta after the collision. The vectors shown in (a) and (b) are equivalent to those in (c); this is indicated by the use of the plus and equal signs, as is common in the mechanics literature. (d) A finger, as a mass-spring-damper system, presses down on the object.

where I denotes the moment of inertia of the object about its mass center and $\mathbf{r}_C$ represents a position vector originating from C to the vector $m\mathbf{v}'$. Both vectors in Eq. (1)–$I\boldsymbol{\omega}$ and $\mathbf{r}_C \times m\mathbf{v}'$–are all perpendicular to the page. Consequently, they must point in opposite directions to cancel each other out. This results in two possible cases: (1) $\boldsymbol{\omega}$ counterclockwise (i.e. negative y-direction) with the moment of $\mathbf{v}'$ about C being clockwise (i.e. positive y-direction); or (2) $\boldsymbol{\omega}$ clockwise with the moment of $\mathbf{v}'$ about C being counterclockwise. The case (2) is physically infeasible due to the impenetrability constraint. Consequently, as indicated in Fig. 2c, the object rotates counterclockwise, while the sense of the moment of $m\mathbf{v}'$ about C is clockwise after the impact.

Finally, successful penetration of the thumb into the space

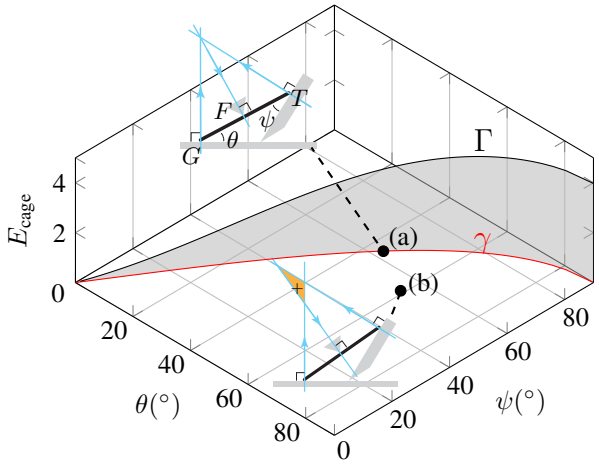

Fig. 3. On the curve γ, the contact normals of the three contacts G, F, and T intersect, where d (see Fig. 2d) is set 0.5 for a unit-length linear object. The three-dimensional curve Γ is given by $\Gamma = (\theta, \psi, E_{\text{cage}})$ where $(\theta, \psi) \in \gamma$ and $E_{\text{cage}} = \frac{1}{2}k\xi^2 + mgz$ as in Eq. (3). All the physical dimensions were removed when computing E_{cage}, where we set $k = 20$, $m = 1$, and $g = 9.81$. ξ and z are simply regarded as the vertical displacement of the contact F and the mass center, collocated at the midpoint of the unit-length object.

beneath the object occurs if the horizontal component of $\mathbf{v}'$ (Fig. 2c) maintains the same direction as $\mathbf{v}$ (Fig. 2a). To ensure this, the horizontal component of the impulse $\mathbf{C}_{\text{avg}}\Delta t$, directed in the negative x-direction, needs to be sufficiently small. One potential approach is to keep the thumb's angle of attack, denoted by α in Fig. 2 (the acute angle formed by the thumb and ground), small. This hypothesis will be tested in our experiments.

B. Post-Strike Caging

Following the event of dynamic thumb strike through which the object is taken off from ground, we establish a mechanism to securely hold the object. See Fig. 2d introducing a finger, rendered as a mass-spring-damper system, making contact on top of the object. When the mechanical impedance of the finger is set sufficiently low, the force $\mathbf{F}$ exerted by the finger becomes non-impulsive (again indicated with a light blue color) and thus will not affect the analysis in Sec. III-A. Accordingly, dynamic thumb penetration can still occur in the presence of the additional finger.

By putting the thumb and finger together, it is possible to effectively suppress the mobility of the object. Specifically, the object can be caged [30], although it is not possible to attain complete immobilization (the first-order mobility index does not vanish with three contacts on the plane [31]). To see this, consider the three-point-contact configuration of the object in Fig. 2d where the object's tips are in contact with the ground at G and the thumb's face at T, along with the finger contact F on its face. We parametrize the configuration of the object-gripper system with θ, ψ, and d as shown in Fig. 2d. The $\theta\psi$-plane shown in Fig. 3 accordingly represents the configuration space when d is fixed. On that plane, we construct the curve $\boldsymbol{\gamma}$, the collection of the configurations at which the three contact normals (note, all the contact normals are well-defined) intersect at a common point (inset (a) of

IEEE Robotics and Automation Letters (RA-L) paper, presented at ICRA 2026, Vienna, Austria. Cite as RA-L paper.

Fig. 3), and consider the configurations "below" the curve (thus with sufficiently large θ). One such configuration is depicted in the inset (b) of Fig. 3. Lemma 1 presented below, an adaptation of Lemma 3 in [32], formalizes that at such configurations as Fig. 3b the object is caged:

Lemma 1. *A linear object is in an energy-bounded cage at configurations with sufficiently large θ, below the curve γ (Fig. 3).*

Proof. See [32]. □

Lemma 1 can be understood as follows. First, the object cannot escape through the gap between the finger and ground (i.e. between G and F) while satisfying the first-order geometry constraints. This can be seen by establishing the feasible twist polytope of the object. In Fig. 3b, the polytope is visualized, by Reuleaux's method [33], as the orange-shaded area (with a "+" label) formed by the contact normals, which can be interpreted as the region of allowable rotation centers. That is, the object is allowed to move only by instantly rotating counterclockwise (as indicated by the + label) around a point in the region, without penetrating the gripper or ground surface. This confirms that it is impossible for the object to slip through the gap between the finger and the ground. Second, although the object can escape the other way, through the gap between the finger and thumb (i.e. between F and T), a positive amount of work needs to be injected against, for example, the force of gravity acting downwards. To sum up, the cages addressed in Lemma 1 enable securely holding the object while scooping it up.

C. Energy Threshold

The energy imparted to the object by the event of thumb strike, i.e. the initial kinetic energy of the object before the collision (see Fig. 2a), has to be high enough for the object to be dynamically lifted by the thumb (Sec. III-A) and to enter a cage (Sec. III-B). The energy threshold E_- can be quantified as

$$E_- = E_{\text{cage}} + E_{\text{loss}} \tag{2}$$

E_{cage} denotes the amount of potential energy for the object to reach a caged configuration such as Fig. 3b from an initial configuration at which $\theta = 0$ (that is, the object rests on the ground surface) while defying the elasticity of the finger's spring and the force of gravity (Fig. 2d):

$$E_{\text{cage}} = \frac{1}{2}k\xi^2 + mgz \tag{3}$$

where ξ and z denote the spring's deformation and the mass center's vertical displacement. Fig. 3 presents an example. The three-dimensional curve Γ is constructed by elevating γ by assigning the value of E_{cage} to each configuration on γ, which can be considered marginally caged. The spatial curve Γ can thus be regarded as a threshold (or "hurdle") of energy to jump over in order to get caged from initial configurations, with zero energy, along the axis $\theta = 0$. In practice, the threshold should be higher due to E_{loss} incorporating various energy losses due to the collision with the thumb, work of frictional forces, and so on. In case of insufficient initial kinetic energy, the object will only be pushed away in a quasidynamic manner.

IV. Implementation of High-Speed Scooping

This section addresses our system to implement the model of high-speed scooping through dynamic manipulation, as detailed in Sec. III, which requires high-speed operation with compliance.

A. Hardware: Direct-Drive Gripper with Swivel Fingertips

Our gripper (Fig. 4a) is the key to realize the manipulation model established in Sec. III. The gripper has two digits and each one is constructed as a five-bar parallel linkage with two degrees-of-freedom (DOF). These digits operate in a fully actuated, direct-drive manner without a gear train, enabling high-speed operation (for dynamic strike by thumb) with active mechanical compliance (for the compliant finger mechanism). Compared to the previous version in [4], our current gripper adopts swivel fingertips with passive compliance for enhanced adaptiveness. See Fig. 4a-b. Specifically, the most distal link of each finger is connected to the five-bar linkage through a revolute joint and a torsional spring. This configuration allows the fingertip to rotate under external perturbations and then return to its original position (its effectiveness will be shown in Sec. V-B3). Therefore, each finger actually has three DOF: two active and one passive. The full up-to-date engineering process for the gripper is available online.[1]

B. Reflex-Based Stiffness Control

To realize dynamic physical interactions, our direct-drive gripper is operated by reflex-based stiffness control (or simplified impedance control), incorporating setpoint feedback motion control with stiffness scheduling:

- Reflex-based: Because the direct-drive gripper can function as a collision sensor due to its 'transparency' [26], we control the gripper to respond reactively to collisions, detected by monitoring joint encoder values (motor current values can also be used).
- Setpoint feedback motion control: More specifically, the gripper, starting from its initial configuration (Fig. 4c), is carried by a motion-controlled arm to strike the ground. This collision triggers the gripper to close to its unique goal configuration where an object can be pinched (Fig. 4c).
- Stiffness scheduling: Before the event of ground strike, the gains of the motion controller (specifically, the ratio between the current into a motor and its shaft's position error) are set sufficiently small in order to compliantly address the impactful physical interaction due to collision. The digits fabricated as a lightweight (33g each) parallel linkage not bearing the weight of the heavy motors of the gripper make this possible by significantly reducing the need for gravity compensation. After the collision, the stiffness values are step-increased in order to securely hold the object.

Specific rollouts of the control strategy are to be provided in our experiments, presented in the next section.

[1] [Online] Hardware project https://github.com/JS-RML/Direct-Drive-Gripper-with-Swivel-Fingertips

IEEE Robotics and Automation Letters (RA-L) paper, presented at ICRA 2026, Vienna, Austria. Cite as RA-L paper.

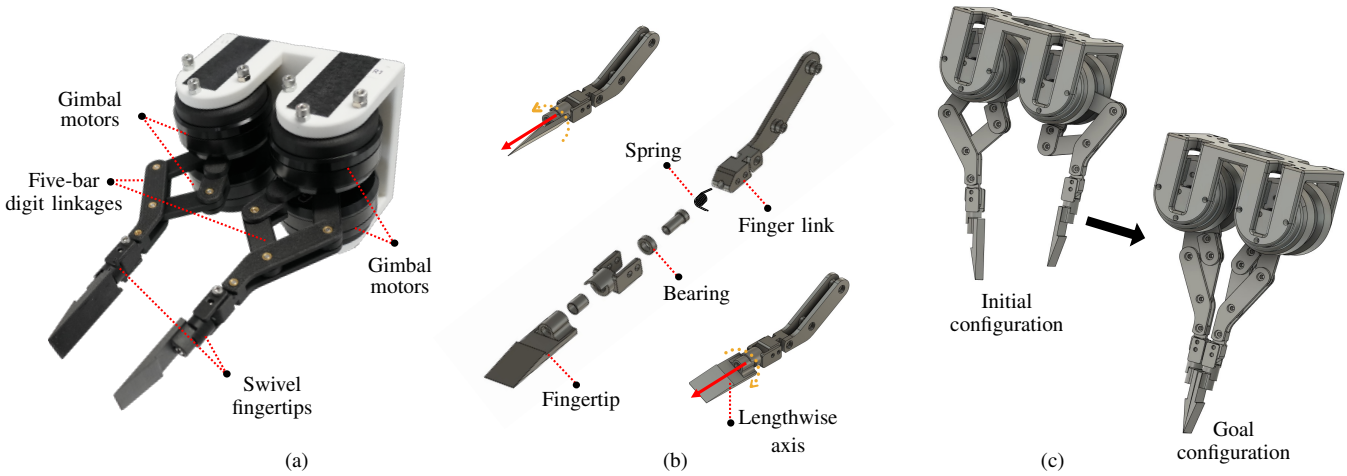

Fig. 4. (a) Our custom two-fingered direct-drive gripper with swivel fingertips. (b) Exploded view of the swivel fingertip. The most distal link can rotate about the lengthwise axis. (c) For the high-speed scooping experiments in this study, the gripper is setpoint-controlled to assume the goal configuration illustrated above. Also refer to the attached video.

V. Experiments

This section provides a series of experiments to validate the model of high-speed scooping discussed in Sec. III. Also refer to the video attachment.

A. Single-Digit Experiments

We begin by testing the dynamic strike model addressed in Sec. III-A. Fig. 5a shows the gripper configured to use only the thumb to strike a 19g rigid plastic card, following the protocol outlined as a two-step sequential procedure below:

- *Ground Collision* (up to the second panel in Fig. 5a): The gripper is moved vertically downward by a robot arm, colliding with the ground at a speed of 0.38m/s, with low motor gain values.
- *Thumb Extension* (from the third panel in Fig. 5a): Upon impact, the thumb is commanded to extend (as also shown in Fig. 4c), with increased motor gains, allowing it to move horizontally and strike the object.

We varied (1) the relative velocity between the thumb and the plastic card v_x, the x-component of $\mathbf{v}$ in Fig. 2a, by adjusting the motion controller's gain values, and (2) the thumb's angle of attack α by adjusting the thumb's initial configurations. In the first case, the thumb's initial configurations remain unaltered; in the second case, the motion controller's gain values remain unchanged. Table I reports the resulting values of v_x', the x-component of $\mathbf{v}'$, and ω_y, the y-component of $\boldsymbol{\omega}$ (refer to Fig. 2c) measured using motion capture equipment. The results confirm that the directions of $\mathbf{v}'$ and $\boldsymbol{\omega}$ align as predicted by the theory in Sec. III-A, enabling the thumb to dynamically penetrate the space beneath the object. Additional key findings include the following: First, penetration is facilitated by a larger initial velocity $\mathbf{v}$, resulting in larger $\mathbf{v}'$ and $\boldsymbol{\omega}$. Second, a smaller angle of attack α makes penetration easier, verifying the hypothesis presented at the end of Sec. III-A.

We also note that the practical outcomes could have deviated from the theory in Sec. III-A due to the complex nature of collision mechanics and potentially unfavorable actual contact geometries. For example, what if reaction $\mathbf{G}$ turns out to be impulsive in the situation of Fig. 2b? Additionally, if a thumb with a realistically blunt (even microscopically) tip collides with an object that also has a blunt tip, the interaction would deviate significantly from the model in Fig. 2, illustrating a collision between a zero-thickness object and an unrounded rigid corner. Nevertheless, the experiments here demonstrate that the theoretical model remains viable despite these unmodeled practical challenges.

TABLE I
Results of Single-Digit Experiments (Object: Plastic Card)

$\mathbf{v}$ experiments (Sec. V-A)		
v_x (m/s)	v_x' (m/s)	ω_y (°/s)
0.36	0.067	−64
0.79	0.302	−314
1.18	0.396	−524
1.51	0.625	−969
α experiments (Sec. V-A)		
α (°)	v_x' (m/s)	ω_y (°/s)
40	0.190	−120
55	0.056	−76
70	0.013	−8

B. Two-Digit Experiments

We now test whether adding an extra digit, creating a two-digit scenario, facilitates successful high-speed scooping through caging, as discussed in Sec. III-B to III-C. The procedure for the two-digit experiments (Fig. 5b) mirrors that of the single-digit experiments (Sec. V-A), with the key difference that we now activate the other digit–the finger–to

IEEE Robotics and Automation Letters (RA-L) paper, presented at ICRA 2026, Vienna, Austria. Cite as RA-L paper.

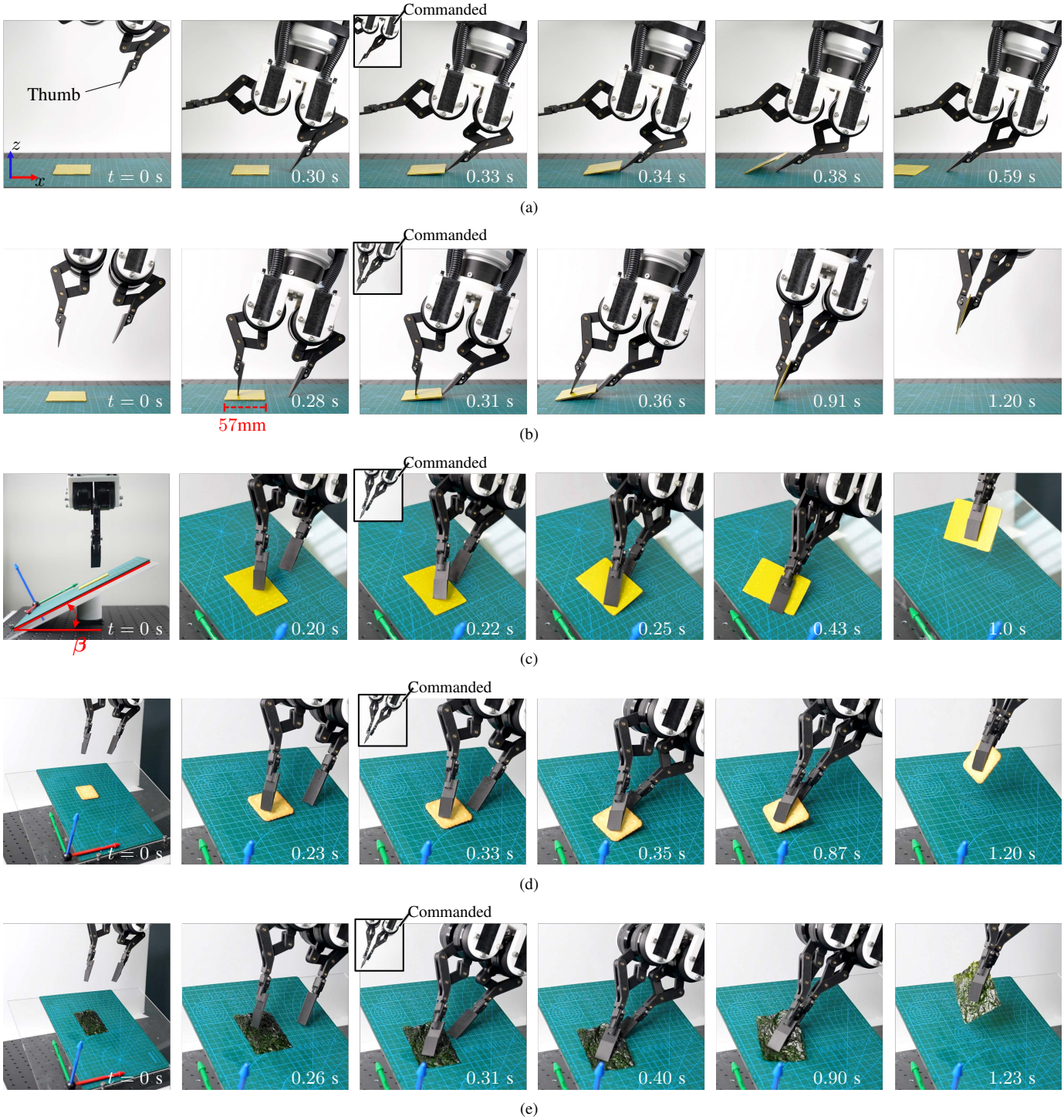

Fig. 5. (a) Single-digit experiment. Only the thumb is activated to make collision with the object, a plastic card. (b) Two-digit experiment. (c) Swivel fingertip experiment on a surface with nonzero β. (d-e) Scooping fragile objects, a cracker (d) and a roasted seaweed snack (e), on a surface with nonzero β by virtue of the swivel fingertips.

make contact on top of the object and command the gripper to fully close upon collision (as also described in Fig. 4c).

1) Setting Parameters: First, we address the challenge of selecting parameters such as α and d (Fig. 2), which relate to the positioning of the thumb and the location of the finger, respectively. If α and d are assumed to remain constant during manipulation, determining their initial values also contributes to planning for high-speed scooping. The energy threshold discussion in Sec. III-C provides an approach to tackle this issue. Specifically, we aim to minimize the energy threshold required to enter a cage, referring to E_{cage} in Eq. (3) (also see Γ in Fig. 3). To achieve this, it is necessary to minimize ξ and z, leading to reducing d (to minimize ξ) and α (to minimize z). In the following experiments, practical considerations of design, kinematics, and control led to minimally setting α and d at 40° and 5mm, respectively, for the plastic card object with a width of 57mm (as also shown in Fig. 5b). Reducing α further would require modifications to the gripper's design and

IEEE Robotics and Automation Letters (RA-L) paper, presented at ICRA 2026, Vienna, Austria. Cite as RA-L paper.

TABLE II
RESULTS OF TWO-DIGIT EXPERIMENTS (OBJECT: PLASTIC CARD)

α experiments (Sec. V-B2)

d (mm)	Thumb attack angle α (°)	(p-gains of finger, p-gains of thumb)		Gripper collides with ground at (m/s)	Success rate
		Before collision	After collision		
15	40	$(20, 20)$	$(50, 100)$	0.38	30/30
15	50	$(20, 20)$	$(50, 100)$	0.38	25/30
15	55	$(20, 20)$	$(50, 100)$	0.38	11/30
15	60	$(20, 20)$	$(50, 100)$	0.38	3/30
15	70	$(20, 20)$	$(50, 100)$	0.38	1/30

***d* experiments (Sec. V-B2)**

d (mm)	Thumb attack angle α (°)	(p-gains of finger, p-gains of thumb)		Gripper collides with ground at (m/s)	Success rate
		Before collision	After collision		
5	55	$(20, 20)$	$(50, 100)$	0.38	30/30
10	55	$(20, 20)$	$(50, 100)$	0.38	23/30
15	55	$(20, 20)$	$(50, 100)$	0.38	11/30
20	55	$(20, 20)$	$(50, 100)$	0.38	0/30
28	55	$(20, 20)$	$(50, 100)$	0.38	0/30

v experiments (Sec. V-B2)

v_x (m/s)	α (°), d (mm)	(p-gains of finger, p-gains of thumb)		Gripper collides with ground at (m/s)	Success rate
		Before collision	After collision		
1.14	55, 15	$(20, 20)$	$(50, 60)$	0.38	0/30
1.40	55, 15	$(20, 20)$	$(50, 80)$	0.38	1/30
1.60	55, 15	$(20, 20)$	$(50, 90)$	0.38	8/30
1.82	55, 15	$(20, 20)$	$(50, 100)$	0.38	11/30
2.03	55, 15	$(20, 20)$	$(50, 110)$	0.38	22/30

Swivel fingertip experiments (Sec. V-B3)

Orientation discrepancy β(°)	Fingertip	(p-gains of finger, p-gains of thumb)		Gripper collides with ground at (m/s)	Success rate
		Before collision	After collision		
15	Swivel	$(20, 20)$	$(40, 60)$	0.38	29/30
	Fixed	$(20, 20)$	$(40, 60)$	0.38	3/30
25	Swivel	$(20, 20)$	$(40, 60)$	0.38	28/30
	Fixed	$(20, 20)$	$(40, 60)$	0.38	0/30

kinematics, specifically the parallel linkage architecture, and a shift from setpoint control to full trajectory control, to ensure that the thumb maintains ground contact all the way at small α values. Similarly, allowing a smaller d would necessitate full trajectory control to keep the finger in contact with the top of the object near its edge. The minimum feasible d would also depend on the object's size, particularly if the object exceeds the gripper's workspace.

2) High-Speed Scooping Experiments: Our experiment results presented in Table II demonstrate that high-speed scooping can be performed with high success using the two-digit configuration, achieving a perfect success rate of 30 out of 30. Each successful high-speed scoop involved dynamic thumb penetration, even in the presence of the finger, followed by subsequent caging, as discussed in Sec. III-B. More specifically, The first two sets of experiments indicate that smaller values of α and d contribute to higher success rates in high-speed scooping, as covered in Sec. V-B1. The third set of experiments in Table II, titled '$\mathbf{v}$ experiments,' shows that higher values of $\mathbf{v}$ lead to more successful high-speed scooping for the same α and d, as discussed in Sec. III-C. These results suggest that the issue of parameter setting–or, more broadly, planning–should be understood as a continuum of success rates rather than a simple success-or-failure decision. In the event of failure, our high-speed approach could help minimize the time lost before a successful scoop.

3) Swivel Fingertip Experiments: In the experiments up to this point, the workplane of the gripper is nominally set perpendicular to the ground surface, as assumed at the beginning of Sec. III. What if this assumption does not hold reasonably true in practice? We now confirm that our swivel fingertips with passive compliance can address this problem. The first panel of Fig. 5c shows the plastic card lying on a plane that is not perpendicular to the gripper's workplane. The orientation discrepancy is denoted as β in the first panel of Fig. 5c. Other conditions remain the same: the gripper is moved vertically downward at a speed of 0.38m/s and is commanded to assume the same goal configuration upon collision with the surface. Table II (the fourth set of experiments) reports the superior performance of the swivel fingertips compared to non-swivel, fixed ones. Upon collision, the swivel fingertips instantly align with the contact surfaces,

IEEE Robotics and Automation Letters (RA-L) paper, presented at ICRA 2026, Vienna, Austria. Cite as RA-L paper.

allowing the thumb to reliably penetrate the space beneath the object, resulting in high success rates. In contrast, fixed fingertips cause failures due to their inability to adapt to the orientation discrepancy. A potential alternative to our swivel fingertip is a needle-like, slender fingertip. This design could address the orientation discrepancy issue without adding a DOF. However, two needle-like fingers might miss each other when closed, potentially reducing the stability of the final pinch grasp. Other problems include the concentrated contact areas leading to higher pressure on specific areas of the object, potentially causing damage.

4) Brittle Objects: Beyond the durable plastic card, we tested brittle objects to assess whether our current system can balance the advantages of dynamic manipulation with the risk of damaging delicate objects. As shown in Fig. 5d-e, it was possible to scoop brittle objects (a cracker and a roasted seaweed snack) using the same setup as in the swivel fingertip experiments in Fig. 5c, with the exception of lowered post-collision gain values: any values between $(10, 10)$ and $(25, 25)$ were successful.

VI. Conclusion and Future Work

In this study, we presented high-speed scooping, a novel dynamic manipulation technique designed for rapidly picking objects up from a hard surface using a multi-fingered gripper. We explored the rigid body dynamics model of high-speed scooping and validated its effectiveness and practicality through extensive experiments. While our direct-drive gripper represents one specific implementation of the model, it can be easily fabricated using off-the-shelf components, suggesting a relatively low entry barrier for gripper technology. Other grippers, provided they offer high speed and compliance, can also be employed. In addition to the feasibility of the rigid body model itself, the success of high-speed scooping is also partly attributed to the conservative nature of the baseline rigid body approach; in other words, non-rigidity and deformation can simplify the handling process to some extent. However, the assumption of negligible thickness (recall Fig. 2) could pose a challenge to its applicability.

As an immediate direction for future work, we are constructing a dataset of high-speed scooping performed with a wide variety of objects, which will support the integration of learning-based methods.

References

[1] N. Correll *et al.*, "Analysis and observations from the first amazon picking challenge," *IEEE Trans. Automat. Sci. Eng.*, vol. 15, no. 1, pp. 172–188, 2018.

[2] A. Hajj-Ahmad, L. Kaul, C. Matl, and M. Cutkosky, "Grasp: Grocery robot's adhesion and suction picker," *IEEE Robot. Automat. Lett.*, vol. 8, no. 10, pp. 6419–6426, 2023.

[3] J. Mahler *et al.*, "Learning ambidextrous robot grasping policies," *Sci. Robot.*, vol. 4, no. 26, 2019.

[4] K. H. Mak, P. Xu, and J. Seo, "High-speed scooping: An implementation through stiffness control and direct-drive actuation," in *2023 IEEE Int. Conf. Robot. Automat. (ICRA)*, 2023, pp. 10 261–10 267.

[5] M. A. Erdmann and M. T. Mason, "An exploration of sensorless manipulation," *IEEE J. Robot. Autom.*, vol. 4, no. 4, pp. 369–379, 1988.

[6] A. Rizzi and D. Koditschek, "Progress in spatial robot juggling," in *Proc. 1992 IEEE Int. Conf. Robot. Automat. (ICRA)*, pp. 775–780.

[7] K. M. Lynch and M. T. Mason, "Dynamic nonprehensile manipulation: Controllability, planning, and experiments," *Int. J. Robot. Res.*, vol. 18, no. 1, pp. 64–92, 1999.

[8] J. Z. Woodruff and K. M. Lynch, "Robotic contact juggling," *IEEE Trans. Robot.*, vol. 39, no. 3, pp. 1964–1981, 2023.

[9] P. Donner and M. Buss, "Cooperative swinging of complex pendulum-like objects: Experimental evaluation," *IEEE Trans. Robot.*, vol. 32, no. 3, pp. 744–753, 2016.

[10] J. Shi *et al.*, "Dynamic in-hand sliding manipulation," *IEEE Trans. Robot.*, vol. 33, no. 4, pp. 778–795, 2017.

[11] A. Zeng *et al.*, "Tossingbot: Learning to throw arbitrary objects with residual physics," *IEEE Trans. Robot.*, vol. 36, no. 4, pp. 1307–1319, 2020.

[12] A. Nazir, P. Xu, and J. Seo, "Rock-and-walk manipulation: Object locomotion by passive rolling dynamics and periodic active control," *IEEE Trans. Robot.*, vol. 38, no. 4, pp. 2354–2369, 2022.

[13] T. McGeer, "Passive dynamic walking," *Int. J. Robot. Res.*, vol. 9, no. 2, pp. 62–82, 1990.

[14] S. H. Collins, M. Wisse, and A. Ruina, "A three-dimensional passive-dynamic walking robot with two legs and knees," *Int. J. Robot. Res.*, vol. 20, no. 7, pp. 607–615, 2001.

[15] C. Jiang, A. Nazir, G. Abbasnejad, and J. Seo, "Dynamic flex-and-flip manipulation of deformable linear objects," in *2019 IEEE/RSJ Int. Conf. Intell. Robots Syst (IROS)*, pp. 3158–3163.

[16] V. Babin and C. Gosselin, "Picking, grasping, or scooping small objects lying on flat surfaces: A design approach," *Int. J. Robot. Res.*, vol. 37, no. 12, pp. 1484–1499, 2018.

[17] C. Eppner *et al.*, "Exploitation of environmental constraints in human and robotic grasping," *Int. J. Robot. Res.*, vol. 34, no. 7, pp. 1021–1038, 2015.

[18] L. Franco *et al.*, "The double-scoop gripper: A tendon-driven soft-rigid end-effector for food handling exploiting constraints in narrow spaces," in *2024 IEEE Int. Conf. Robot. Automat.*, pp. 4170–4176.

[19] E. Turco *et al.*, "Grasp planning with a soft reconfigurable gripper exploiting embedded and environmental constraints," *IEEE Robot. Automat. Lett.*, vol. 6, no. 3, pp. 5215–5222, 2021.

[20] A. Billard and D. Kragic, "Trends and challenges in robot manipulation," *Science*, vol. 364, no. 6446, 2019.

[21] H. Liang, X. Lou, Y. Yang, and C. Choi, "Learning visual affordances with target-orientated deep q-network to grasp objects by harnessing environmental fixtures," in *2021 IEEE Int. Conf. Robot. Automat. (ICRA)*, pp. 2562–2568.

[22] D. Wang *et al.*, "Multi-stage reinforcement learning for non-prehensile manipulation," *IEEE Robot. Automat. Lett.*, vol. 9, no. 7, pp. 6712–6719, 2024.

[23] H. Asada and K. Youcef-Toumi, *Direct-drive robots: theory and practice*. MIT press, Cambridge, MA, 1987.

[24] S. Wang, A. Bhatia, M. T. Mason, and A. M. Johnson, "Contact localization using velocity constraints," in *2020 IEEE/RSJ Int. Conf. Intell. Robots Sys. (IROS)*, pp. 7351–7358.

[25] M. Ebner and R. Wallace, "A direct-drive hand: design, modeling and control," in *IEEE Int. Conf. Robot. Automat.*, 1995, pp. 1668–1673.

[26] A. Bhatia, A. M. Johnson, and M. T. Mason, "Direct drive hands: Force-motion transparency in gripper design," in *Robot.: Sci. Syst.*, 2019.

[27] G. Kenneally, A. De, and D. E. Koditschek, "Design principles for a family of direct-drive legged robots," *IEEE Robot. Automat. Lett.*, vol. 1, no. 2, pp. 900–907, 2016.

[28] D. V. Gealy *et al.*, "Quasi-direct drive for low-cost compliant robotic manipulation," in *2019 Int. Conf. Robot. Automat.*, pp. 437–443.

[29] N. Hogan, "Impedance Control: An Approach to Manipulation: Part II—Implementation," *J. Dyn. Syst., Meas., Control*, vol. 107, no. 1, pp. 8–16.

[30] J. Mahler *et al.*, "Energy-bounded caging: Formal definition and 2-d energy lower bound algorithm based on weighted alpha shapes," *IEEE Robot. Automat. Lett.*, vol. 1, no. 1, pp. 508–515, 2016.

[31] E. Rimon and J. Burdick, "Mobility of bodies in contact. I. a 2nd-order mobility index for multiple-finger grasps," *IEEE Trans. Robot. Automat.*, vol. 14, no. 5, pp. 696–708, 1998.

[32] K. H. Mak, C. H. Kim, and J. Seo, "Robust ungrasping of high aspect ratio objects through dexterous manipulation," *IEEE Robot. Automat. Lett.*, vol. 7, no. 2, pp. 2843–2850, 2022.

[33] M. T. Mason, *Mechanics of robotic manipulation*. MIT press, 2001.